Journal of Inclusion Phenomena and Macrocyclic Chemistry **36:** 163–178, 2000.

A Kinetic Study of the Dehydration of $VOPO_4.2H_2O$ by Thermal Methods

L. BENEŠ[1]⋆, E. ČERNOŠKOVÁ[1], J. MÁLEK[1], K. MELÁNOVÁ[1], P. PATRONO[2] and V. ZIMA[1]

[1] *Joint Laboratory of Solid State Chemistry of the Academy of Sciences of the Czech Republic and University of Pardubice, Studentská 84, 532 10 Pardubice, Czech Republic;* [2] *IMAI-CNR, Area della Ricerca di Roma, Via Salaria km 29,300, C.P. 10 00016 Monterotondo Scalo, Rome, Italy.*

(Received: 20 October 1998; in final form: 26 January 1999)

Abstract. The dehydration of $VOPO_4.2H_2O$ has been studied by thermogravimetric analysis (TGA), differential thermal analysis (DTA) and differential scanning calorimetry (DSC). From the shift of the DTA, DTG, and DSC peaks, activation energies of the dehydration processes have been calculated based on Kissinger's method. The most suitable kinetic models for two-step dehydration have been found.

Key words: vanadium phosphate, thermal methods, mechanism of dehydration, intercalate.

1. Introduction

As emphasized by Schöllhorn [1], most studies done in the field of solid-state chemistry are focused on the synthesis of new materials and their static description, i.e., geometrical and electronic structure and physical properties. Less attention is paid, however, to the reactivity of solids or to kinetic aspects connected with these materials. In this paper, we would like to contribute to this topic by studying the dehydration of $VOPO_4{\cdot}2H_2O$ as a model system.

Vanadium phosphates exhibit a wide range of structures due to the different oxidation states of vanadium V(V), V(IV) or V(III) respectively and the variety of ways in which phosphate tetrahedra and vanadium polyhedra can be condensed through shared corners, edges, or faces. A relatively simple example of two-dimensional vanadium phosphate is $VOPO_4{\cdot}2H_2O$. The structure of $VOPO_4{\cdot}2H_2O$ is layered tetragonal (a = 6.20 Å, c = 7.41 Å) with space group P4/nmm as determined by XRD [2]. The space group P4/n was found by neutron diffraction which takes into account the positions of hydrogen atoms [3]. The layers are built up of corner sharing VO_6 octahedra and PO_4 tetrahedra. Four equatorial oxygens of the VO_6 octahedron are shared by phosphorus, one of the axial oxygens is a vanadyl oxygen, and the second one belongs to a water molecule coordinated to vanadium. The second water molecule is bonded by a weak H-bridge between layers. The

⋆ Author for correspondence.

thermal dehydration of layered $VOPO_4 \cdot 2H_2O$ near 400 °C under $p(O_2) = 101.3$ kPa [4] leads to α_I-$VOPO_4$ (a = 6.20 Å, c = 4.18 Å), whose cell parameters are slightly different from those of the previously known α-$VOPO_4$ obtained by heating of the mixture of oxides which is now called α_{II}-$VOPO_4$ (a = 6.014 Å, c = 4.434 Å) [5]. The structure of the layers in α_I-$VOPO_4$ is the same as in $VOPO_4 \cdot 2H_2O$.

The interlayer water is released in two steps during heating of $VOPO_4 \cdot 2H_2O$. The first molecule of water is liberated at 44 °C producing the monohydrate with c = 6.3 Å as observed by XRD and thermomechanical analysis [6]. The second dehydration step occurs at 80 °C. The temperatures of dehydration obtained from TG-DTA are slightly higher [7]. This difference can be explained by the insensitivity of TG to crystal structure changes which occur during release of water from the interlayer space before its evaporation from the sample. In contrast to dehydration, the intercalation of water does not proceed via the formation of $VOPO_4 \cdot H_2O$ [8]. A reaction mechanism was proposed, based on the shifts of the positions and the widths of the (00l) lines. The formation of a Hendricks–Teller disordered layered lattice was presumed, composed of α_I-$VOPO_4$ and $VOPO_4 \cdot 2H_2O$ layers [8].

This paper gives the results of the study of the kinetics of dehydration of $VOPO_4 \cdot 2H_2O$ using TG, DTA and DSC.

2. Kinetic Analysis

It is usually assumed that the basic kinetic equation for solid state processes under non-isothermal conditions can be expressed as a function of the fractional conversion α ($0 < \alpha < 1$) in the following form [9]:

$$\left(\frac{\mathrm{d}\alpha}{\mathrm{d}t}\right) = A \cdot \exp(-E_a/RT) \cdot f(\alpha), \tag{1}$$

where A is a pre-exponential factor of the Arrhenius type rate constant and E_a is the apparent activation energy. The function $f(\alpha)$ in Equation (1) is an analytical expression describing the kinetic model of the solid state reaction (Table I). It is well known that the kinetic parameters A and E_a in Equation (1) are mutually correlated [10–12]. Therefore, it is practically impossible to determine all kinetic parameters by conventional non-linear regression algorithms of a single non-isothermal curve. This problem can be solved by calculating the apparent activation energy, E_a, from several non-isothermal curves.

A very simple method of calculation of activation energy is based on a logarithmic form of Equation (1):

$$\ln\left(\frac{\mathrm{d}\alpha}{\mathrm{d}t}\right) = \ln[A \cdot f(\alpha)] - \frac{E_a}{RT}. \tag{2}$$

The slope of $\ln(\mathrm{d}\alpha/\mathrm{d}t)$ versus $1/T$ plot (for constant α) obtained from TA data for different heating rates gives the value of the apparent activation energy. This

Table I. The kinetic models and maxima of the $z(\alpha)$ function (α_p^∞) and the $y(\alpha)$ function (α_M)

Model	Symbol	$f(\alpha)$	α_p^∞	α_M
Reaction order	RO(n)	$(1-\alpha)^n$	$1-n^{1/(1-n)}$	0
Johnson–Mehl–Avrami	JMA($m>1$)	$m(1-\alpha)\cdot[-\ln(1-\alpha)]^{1-1/m}$	0.633	$1-\exp\left(\frac{1}{m}-1\right)$
Šesták–Berggren	SB(M, N)*	$\alpha^M(1-\alpha)^N$	$>\alpha_M$	$\frac{M}{M+N}$
2D-phase boundary reaction	R2	$(1-\alpha)^{1/2}$	0.750	0
3D-phase boundary reaction	R3	$(1-\alpha)^{2/3}$	0.704	0
2D-diffusion	D2	$-1/\ln(1-\alpha)$	0.834	0
Jander Eq.	D3	$\frac{3(1-\alpha)^{2/3}}{2[1-(1-\alpha)^{1/3}]}$	0.704	0
Ginstling–Brounshtein Eq.	D4	$\frac{3}{2[(1-\alpha)^{-1/3}-1]}$	0.776	0

* The SB model is valid for $0<M<1$ (see Ref. [16]).

procedure can be repeated for various values of α. The E_a should be invariant with respect to α in the $0.3 < \alpha < 0.7$ range. Another method of calculating the apparent activation energy, which is known as Kissinger's method [13], is based on the condition for the maximum of the peak ($d^2\alpha/dt^2 = 0$) defined by Equation (1):

$$\ln\left(\frac{\beta}{T_p^2}\right) = \ln\left[-\left(\frac{df(\alpha)}{d\alpha}\right)_{\alpha_p} \cdot \frac{AR}{E_a}\right] - \frac{E_a}{RT_p}, \tag{3}$$

where T_p and α_p is the peak temperature and the fractional conversion, respectively, and β is the heating rate. The activation energy is then calculated from the slope of the $\ln(\beta/T_p^2)$ vs. $1/T_p$ dependence. In fact, the first term on the right-hand side of Equation (3) is constant only for a first order process, i.e. $f(\alpha) = 1 - \alpha$, because in this case $df(\alpha)/d\alpha = -1$. Nevertheless, it was shown [14] that the error in the activation energy determined by this method does not exceed 5% for other kinetic models.

The kinetic model can be determined using the $y(\alpha)$ and $z(\alpha)$ function obtained by a simple transformation of non-isothermal data [11, 12, 15]:

$$y(\alpha) = \left(\frac{d\alpha}{dt}\right) \cdot \exp(-E_a/RT), \tag{4a}$$

$$z(\alpha) \approx \left(\frac{d\alpha}{dt}\right) \cdot T^2. \tag{4b}$$

For practical reasons these functions are normalized within the $\langle 0, 1\rangle$ interval. It was shown by Málek [12] that the maximum of the $z(\alpha)$ function (usually labeled α_p^∞) has characteristic values for basic kinetic models as shown in Table I. It is seen that α_p^∞ is constant for the R2, R3, D2, D3, D4 and JMA(m) models. On the other hand it depends on the particular value of the kinetic exponent for the RO(n) or SB(M, N) model. Similar rules can be formulated for the $y(\alpha)$ function [11, 12]:

1. If the $y(\alpha)$ function has a maximum at $\alpha_M = 0$ then it can be convex, linear or concave. The convex dependence corresponds to the RO($n < 1$) model, the linear dependence to the JMA($m = 1$) or RO($n = 1$) model (these two models are formally identical) and the concave dependence to the JMA($m < 1$), D2, D3, D4 and RO($n > 1$) models.
2. If the $y(\alpha)$ function exhibits a maximum in the interval of $\alpha_M \in (0, \alpha_p)$ (where α_p is the fractional extent of reaction at the maximum $d\alpha/dt$) then it corresponds to the SB(M, N) or JMA($m > 1$) model. The mathematical conditions for these maxima are shown in Table 1.

Thus, the shape of both the $y(\alpha)$ and $z(\alpha)$ functions can be used conveniently for the determination of the most probable kinetic model [12] for solid state processes.

For the dehydration of solids, the following presumptions can be established [17]:

(i) The reaction most probably starts on surface sites with structural defects such as dislocations, corners, impurities, or superficial damage. In this way, point areas containing product are formed. Such a process is called "nucleation".
(ii) Subsequent chemical reaction occurs mostly within an interfacial zone – in an area between reactant and product phases.
(iii) The product embedded in the reactant is therefore surrounded by an advancing interface where chemical change proceeds. In such a way, a "growth" process is established. In two-dimensional systems, the interface has a circular shape with increasing radius.
(iv) Continued growth results in acceleration of the reaction rate to the point when the nuclei begin to merge so that interface expansion becomes decelerated. Before completion, the interface area forms a single shell migrating toward the center of the particle.

3. Experimental

Vanadyl phosphate dihydrate was prepared according to the Ladwig method [7] by refluxing a suspension of V_2O_5 in diluted H_3PO_4. The prepared polycrystalline yellow solid was sieve analysed and the fraction with particle size of 0.1–0.2 mm was used for the study.

The thermal behavior of the material was recorded on a Stanton Redcroft STA-801 model simultaneous TG-DTA thermoanalyzer with ignition up to 250 °C (heating rate of 2, 5, 10, 15, and 20 °C min^{-1}, Pt crucibles, Pt–Pt/Rh thermocouples) in nitrogen flow (30 l min^{-1}).

DSC experiments were performed using a Mettler DSC12E instrument. The instrument was previously calibrated with indium, tin and lead standards (E_{In} = 1118.75 units mW^{-1}, τ_{lag} = 15 s). Crystalline powder samples of about 1 mg were placed in open aluminum pans and measured with selected heating rates (2–20 K min^{-1}) in the range from 20 to 180 °C. As an atmosphere, a flow of wetted nitrogen was used, with relative humidities 0–76% and with a flow rate of approx. 30 l min^{-1}. Nitrogen with desired relative humidity (r.h.) was generated by bubbling dry gas through the saturated solution of LiCl (r.h. = 11%), $CH_3COOK{\cdot}1.5H_2O$ (22%), $MgCl_2{\cdot}6H_2O$ (33%), $K_2CO_3{\cdot}2H_2O$ (43%), $NaBr{\cdot}2H_2O$ (58%), NaCl (76%).

4. Results and Discussion

The thermal dehydration of $VOPO_4{\cdot}2H_2O$ under non-isothermal conditions was studied by DSC and by the simultaneous TG-DTA technique. Figure 1 shows a typical thermal dehydration TG curve for the $VOPO_4{\cdot}2H_2O$ sample. Two dehydration steps corresponding to the deintercalation of two molecules of water are clearly separated. The agreement of the calculated (dashed lines) and observed (solid line) weight loss of water is very good taking into account the fact that the removal of

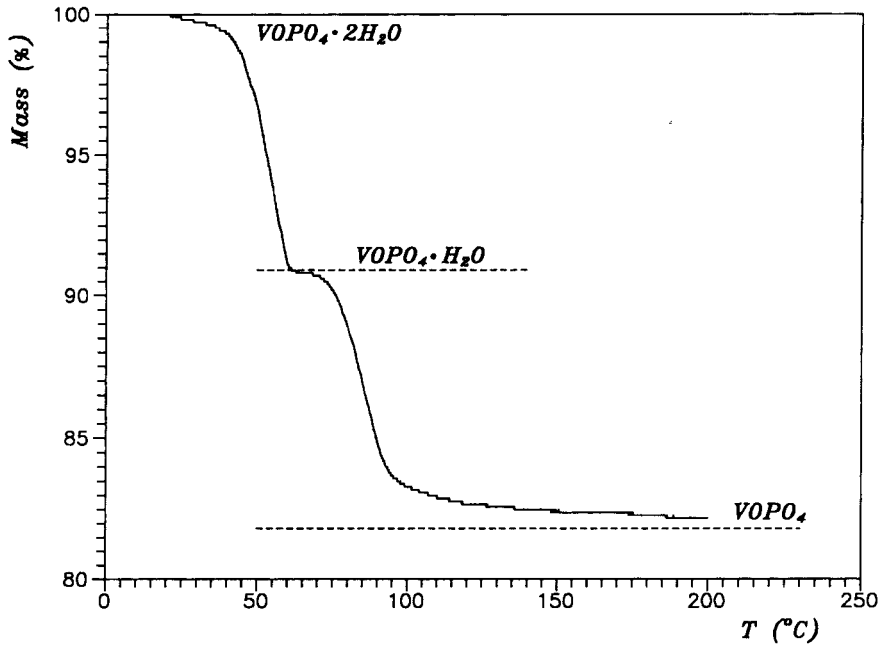

Figure 1. TG curve corresponding to the thermal dehydration of the $VOPO_4 \cdot 2H_2O$ sample (≈11 mg) in a dry nitrogen atmosphere. Calculated mass losses corresponding to the release of two molecules of water are marked by the dashed lines.

the last traces of water might be a very slow process and, therefore, the calculated limit (81.8%) is not reached below 200 °C even when a very slow heating rate (1 $K \cdot min^{-1}$) is used. These two dehydration steps become partially overlapped at higher heating rates as evident in Figure 2 where the results of simultaneous DTA-DTG experiments are shown. The apparent activation energy, E_a, can be calculated using Kissinger's method from the temperature shift of the peaks corresponding to these two dehydration steps (see Figure 3). The results are summarized in Table II. It seems that the apparent activation energies are very close (within the limits of experimental errors) for both processes. Due to partial overlapping of two dehydration steps it is practically impossible to make a kinetic analysis based on the $y(\alpha)$ and $z(\alpha)$ functions as described in Section 2.

Figure 4 shows DSC curves for the thermal dehydration of a $VOPO_4 \cdot 2H_2O$ sample measured in a dry nitrogen atmosphere at five different heating rates. The apparent activation energies, E_a, calculated using Kissinger's method for the two dehydration steps are summarized in Table 2. In this case, the values of E_a are higher than those obtained from DTA and DTG data. These discrepancies are probably due to the differences in the sample mass used in both techniques (1 mg and 11 mg, respectively) as well as due to the different geometries of the measurement cells. The advantage of the DSC technique in this case is that the resolution of the thermal effects corresponding to the two dehydration steps is better than that for the

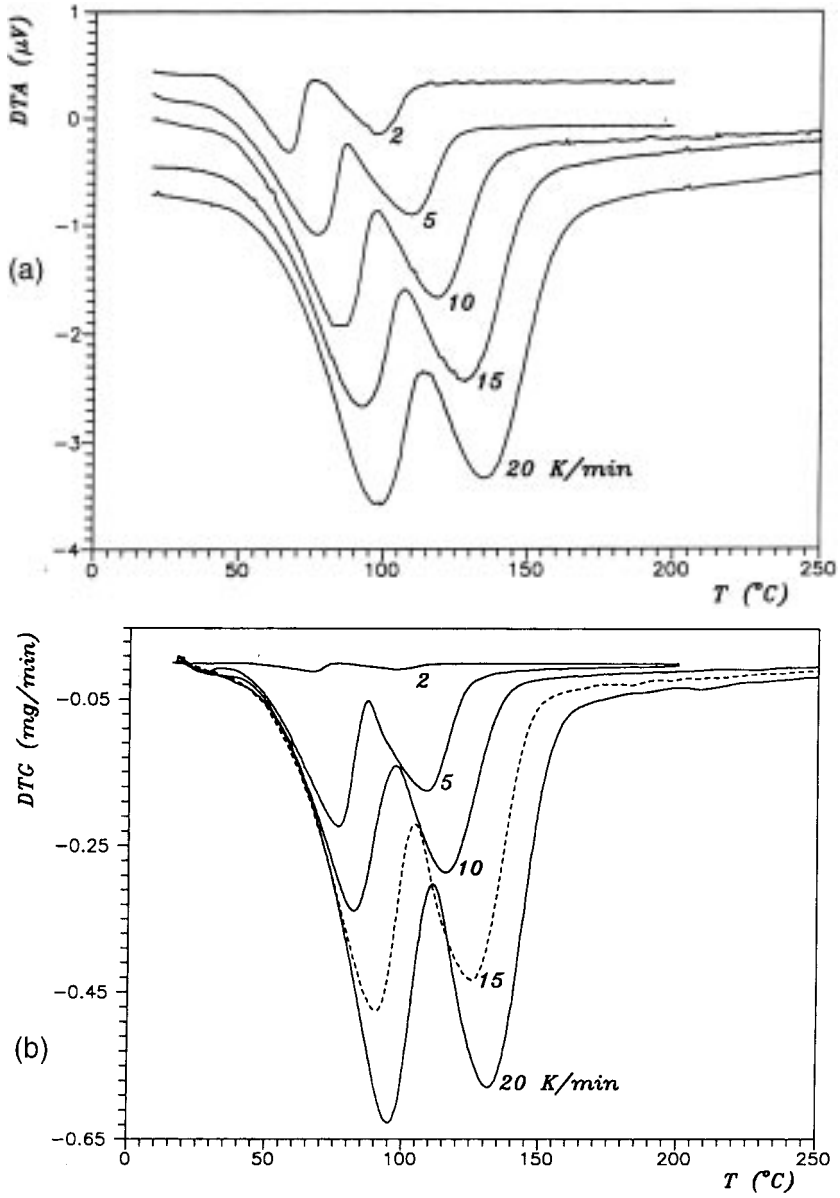

Figure 2. Simultaneous DTA (a) and DTG (b) curves of the $VOPO_42H_2O$ sample (≈12 mg) in a dry nitrogen atmosphere. The different heating rates are indicated.

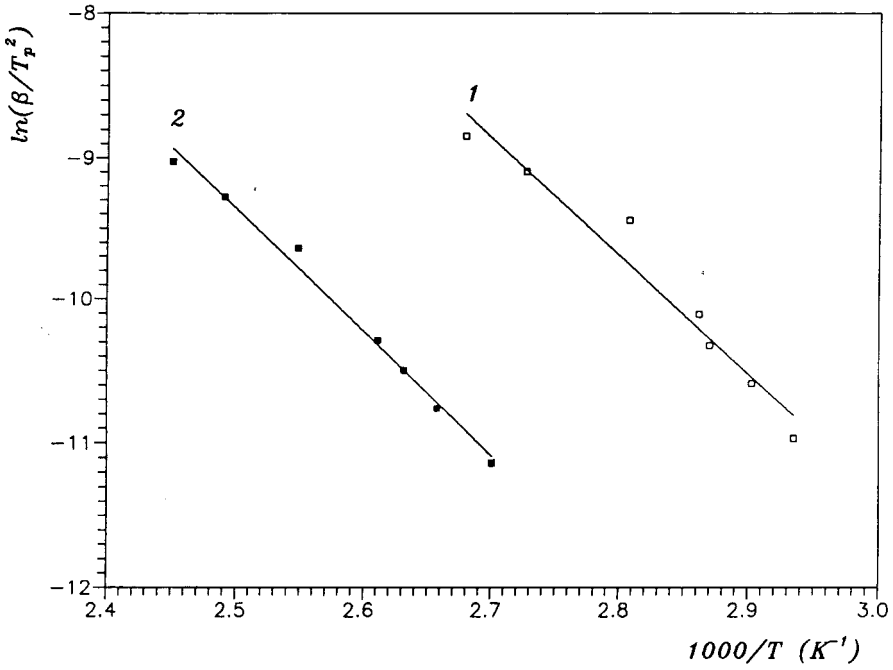

Figure 3. Kissinger's plot for the first (1) and second (2) dehydration peak of the $VOPO_4 \cdot 2H_2O$ sample shown in Fig. 2a.

Table II. Activation energy calculated by Kissinger's method for different experimental data

Data	E (kJ mol^{-1})	
	Peak #1	Peak #2
DSC	90 ± 7	94 ± 10
DTG	80 ± 6	77 ± 6
DTA	69 ± 6	72 ± 3

simultaneous DTA-TG experiment. Therefore, it is possible to calculate the fractional conversion for both dehydration steps and subsequently the isoconversional analysis as well as the analysis based on the $y(\alpha)$ and $z(\alpha)$ functions can be performed. Figure 5 shows the apparent activation energies as a function of fractional conversion calculated by the isoconversional method described in Section 2. The values of E_a in the $0.3 < \alpha < 0.7$ range were found to be 92 ± 7 and 82 ± 8 kJ mol^{-1} for the first and second dehydration step, respectively. These values are in reasonable agreement with the results obtained by Kissinger's method (see Table II).

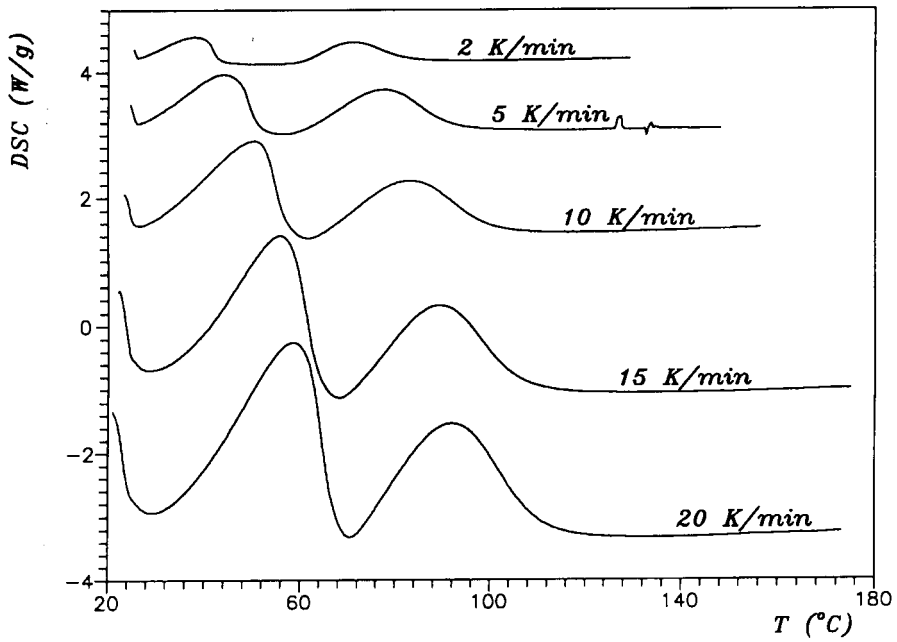

Figure 4. DSC curves obtained during heating of the $VOPO_4 \cdot 2H_2O$ sample (≈1 mg) in a dry nitrogen atmosphere. The different heating rates are indicated.

The values of the apparent activation energy are very close for both steps of the dehydration regardless of the methods used for their determination. It should be pointed out that the values of E_a are within the interval (90 ± 20 kJ mol^{-1}) for dehydration of many inorganic salts [18]. It seems therefore that the highest contribution to the value of E_a is evaporation of water from the surface of the crystals. This is also supported by the fact that the DSC measurements reflect evaporation of water from the sample surface rather than a release of water from the interlayer space (see Introduction).

The functions $y(\alpha)$ and $z(\alpha)$ calculated for both dehydration steps using Equations (4a) and (4b) are shown in Figures 6 and 7. It is evident that both these functions are practically invariant with respect to heating rates for the second dehydration step. On the other hand there is a marked influence of the heating rate on the $y(\alpha)$ and $z(\alpha)$ functions for the first dehydration step. This probably indicates that the first step of dehydration is a more complex process (composed probably of several overlapping steps) in comparison with the removal of the second molecule of water. The maxima of these functions, α_M and α_p^{∞}, are summarized in Table III. It seems that the first dehydration step probably corresponds to the phase boundary controlled reaction. In contrast, the second dehydration step can be described by a two-parameter SB model which probably corresponds to an autocatalytic process.

The rate expression corresponding to the first dehydration step is probably controlled by diffusive migration of water to the crystal edge or reaction interface,

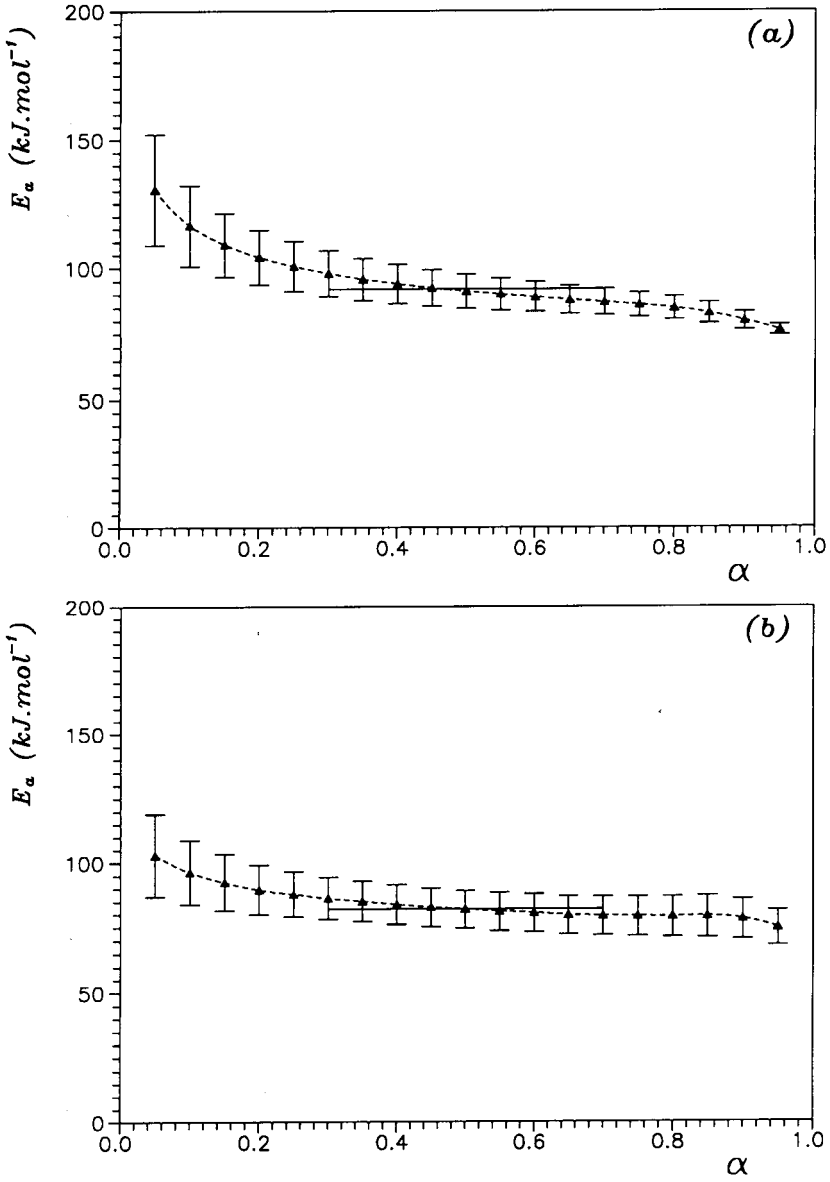

Figure 5. Activation energy as a function of fractional conversion α calculated by the isoconversional method. (a) the first dehydration peak, (b) the second dehydration peak in Figure 1. Dotted lines are drawn to guide the eye and full lines corresponds to the average value of activation energy in the $0.3 < \alpha < 0.7$ range.

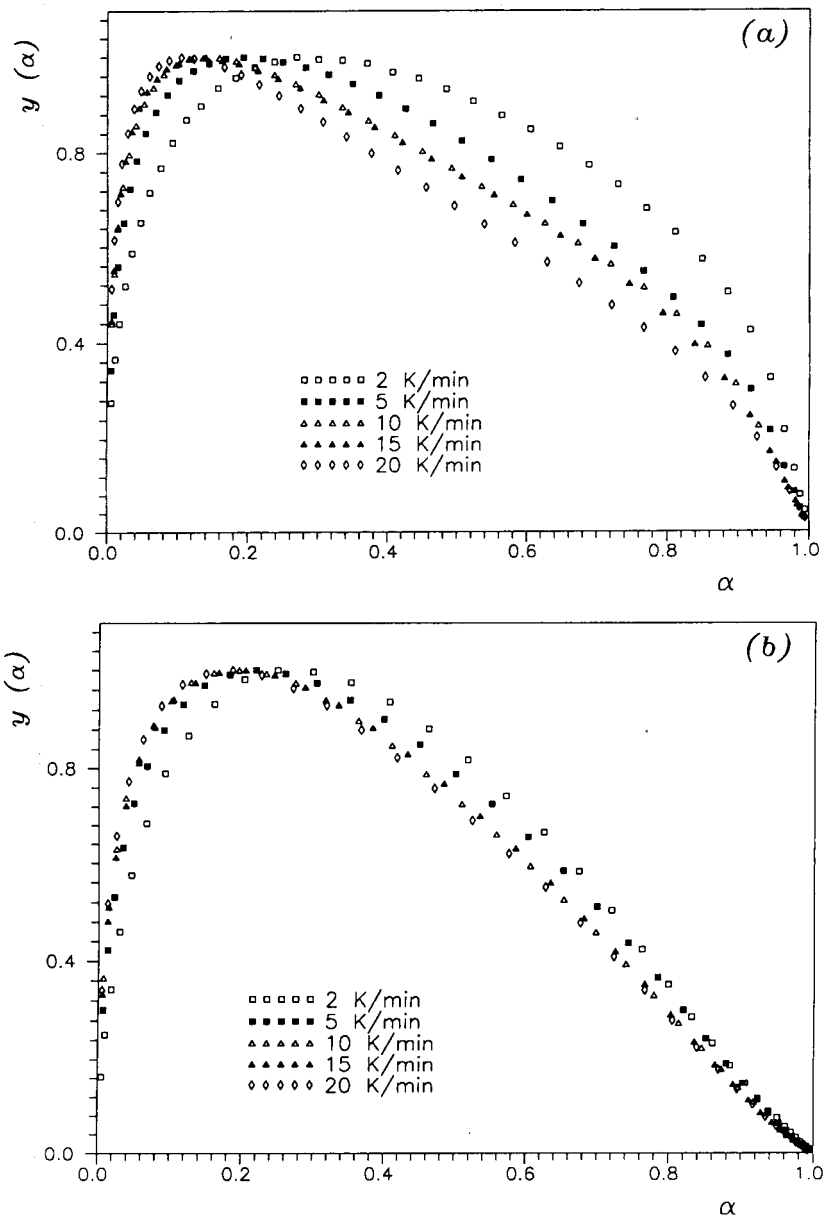

Figure 6. Normalized $y(\alpha)$ functions corresponding to the first dehydration peak (a) and the second dehydration peak (b) of the $VOPO_4 \cdot 2H_2O$ sample shown in Figure 4.

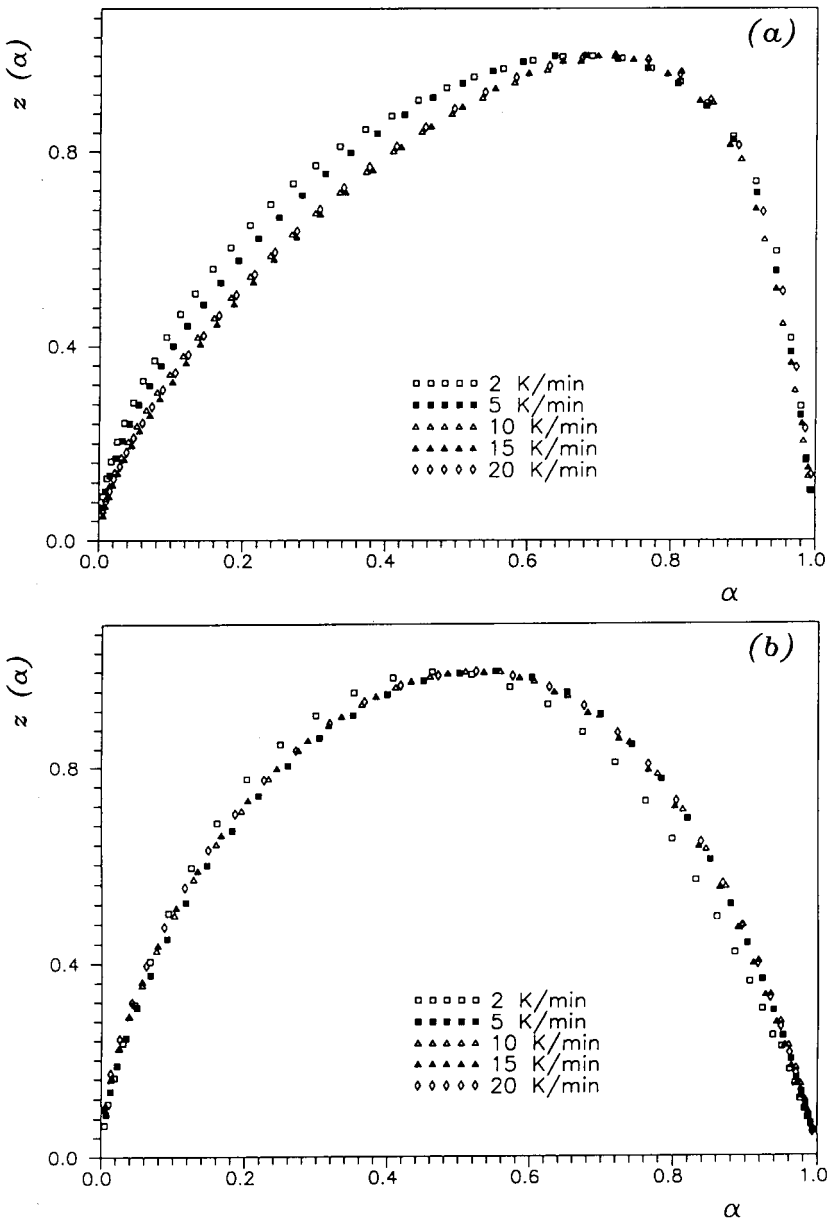

Figure 7. Normalized $z(\alpha)$ functions corresponding to the first dehydration peak (a) and the second dehydration peak (b) of the $VOPO_4 \cdot 2H_2O$ sample shown in Figure 4.

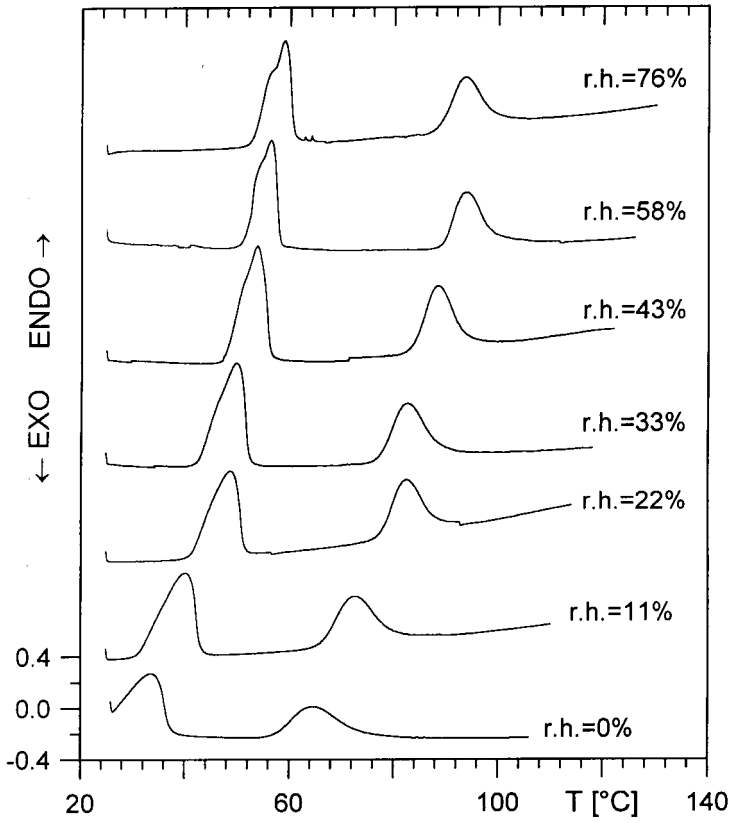

Figure 8. DSC curves obtained during heating of the $VOPO_4 \cdot 2H_2O$ sample (≈1 mg) at different relative humidities of the nitrogen atmosphere. Heating rate: 1 K min^{-1}.

Table III. The maxima of the $y(\alpha)$ and $z(\alpha)$ functions, corresponding to DSC data obtained in a dry nitrogen atmosphere

Maximum	Peak #1	Peak #2
α_M	0.24 ± 0.08	0.21 ± 0.03
α_p^∞	0.70 ± 0.03	0.52 ± 0.02

possibly including a contribution from geometric factors [18, 19]. This is consistent with a relatively high value of α_p^∞ observed for the first dehydration peak. The more strongly bonded first water molecule which is coordinated to the vanadium atom is released in the second step. The higher energy requirement for the release of the water is compensated by an energy contribution from a new bond formed by the coordination of vanadium atoms to oxygens of the vanadyl groups of neighboring layers. This process causes a greater decrease of the interlayer space. As the

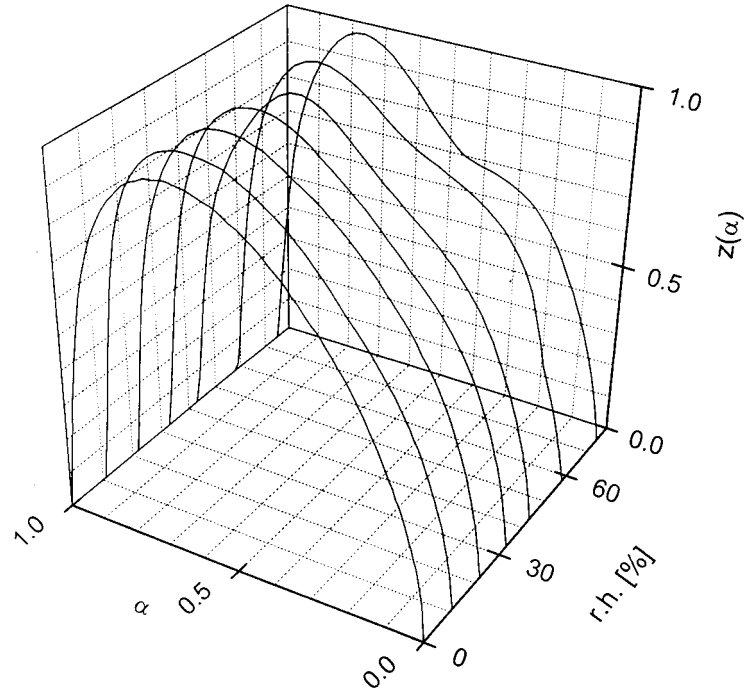

Figure 9. Normalized $z(\alpha)$ functions corresponding to the DSC data at different relative humidities of the nitrogen atmosphere for the first dehydration peak in Figure 8.

$(VOPO_4)_\infty$ layers have limited flexibility, the decrease of the basal spacing near one coordination site generates steric tension in the neighboring coordination sites occupied by water molecules. Consequently, the water molecules in the neighborhood of an empty – deintercalated – site also tends to deintercalate. So, the rate of deintercalation increases with the increasing number of deintercalated sites in the neighborhood of the intercalated sites. This phenomenon can be considered as a reverse case of the process described by Alberti [20] for intercalation of zirconium phosphate by metal ions. A considerable increase in defect density after the first dehydration step is presumed to be due to the change in the crystal dimensions caused by the changes of the interlayer distance. Therefore a large number of nuclei may be formed on the greater surface area available per unit weight of the solid. As a consequence of this process a lower value of α_p^∞ is expected [21]. This was confirmed experimentally for the second dehydration peak (see Table III).

The influence of humidity on the dehydration kinetics was studied by using DSC in a nitrogen atmosphere. The DSC curves are shown in Figure 8 for relative humidity in the 0–76% range. It is seen that both dehydration processes are shifted to higher temperature with increasing relative humidity. In addition, at higher humidities (r.h. $>43\%$), a more complex dehydration process takes place as indicated by the occurrence of a shoulder at this peak.

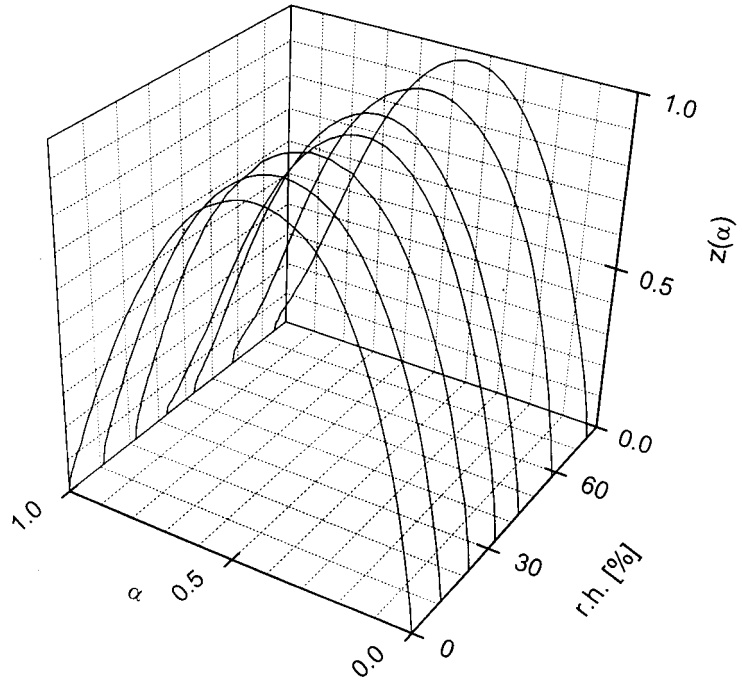

Figure 10. Normalized $z(\alpha)$ functions corresponding to the DSC data at different relative humidities of the nitrogen atmosphere for the second dehydration peak in Figure 8.

Figures 9 and 10 show the effect of the relative humidity on the shape of the $z(\alpha)$ function. The maximum α_p^∞ of this function practically does not change with the relative humidity for both steps and, therefore, it seems that the dehydration mechanism remains practically unchanged. Nevertheless, it is evident that there is a shoulder which becomes more pronounced at higher relative humidity in the case of the first dehydration process. This fact clearly indicates a more complex dehydration mechanism composed probably of several overlapping steps as anticipated above.

5. Conclusions

Using the method described above, and with the knowledge of geometrical and electronic structure, it is possible to describe processes taking place in solids, which are initiated and influenced by temperature changes.

Dehydration of $VOPO_4 \cdot 2H_2O$ proceeds in two steps which differ in their mechanisms. The first step, the release of weakly bonded second water molecules (see Introduction), is influenced by several factors. These factors include the breaking of weak H-bonds to phosphate oxygens and overcoming the energy barrier during migration of these molecules from the interlayer space of vanadyl phosphate. The second step of dehydration consists of the release of water coordinated to vana-

dium. Consequent formation of V=O–V=O bonds can serve as a driving force for the further deintercalation of water. From another point of view, this type of reaction can be considered as an autocatalytic reaction. The position of the dehydration peaks measured by DSC is influenced by the humidity of the atmosphere used.

Acknowledgment

This work was carried out in the framework of the Agreement for scientific cooperation between the National Research Council of Italy and the Academy of Sciences of the Czech Republic. The Czech authors wish to thank the Grant Agency of the Czech Republic (Grant No. 203/97/1010) and the Academy of Sciences of the Czech Republic (Key Project No. 12) for financial support. The DSC 12E instrument used for our measurements was donated by courtesy of the ANATECH B. V. company.

References

1. R. Schöllhorn: *Angew. Chem. Int. Ed. Engl*. **35**, 2338 (1996).
2. H. R. Tietze: *Aust. J. Chem.* **34**, 2035 (1981).
3. M. Tachez, F. Theobald, J. Bernard, and A. W. Hewat: *Rev. Chim. Miner.* **19**, 291 (1982).
4. E. Bordes, P. Courtine, and G. Pannetier: *Ann. Chim.* **8**, 105 (1973).
5. B. Jordan and C. Calvo: *Can. J. Chem.* **51**, 2621 (1973).
6. V. Zima, L. Beneš, J. Málek, and M. Vlček: *Mat. Res. Bull.* **29**, 687 (1994).
7. G. Ladwig: *Z. Anorg. Allg. Chem.* **338**, 266 (1965).
8. L. Beneš and V. Zima: *J. Incl. Phenom.* **20**, 381 (1995).
9. J. Šesták: *Thermophysical Properties of Solids, Their Measurements and Theoretical Analysis*, Elsevier, Amsterdam (1984).
10. J. Málek and V. Smrčka: *Thermochim. Acta* **186**, 153 (1991).
11. J. Málek: *Thermochim. Acta* **138**, 337 (1989).
12. J. Málek: *Thermochim. Acta* **200**, 257 (1992).
13. H. E. Kissinger: *Anal. Chem*. **29**, 1702 (1957).
14. J. M. Criado and A. Ortega: *J. Non-Cryst. Solids* **87**, 302 (1986).
15. J. Málek: *Thermochim. Acta* **267**, 61 (1995).
16. J. Málek, J. M. Criado, J. Šesták, and J. Militký: *Thermochim. Acta* **153**, 429 (1989).
17. H. Tanaka, N. Koga, and A. K. Galwey: *J. Chem. Educ.* **72**, 251 (1995).
18. A. K. Galwey: *J. Therm. Anal*. **38**, 99 (1992).
19. M. E. Brown, D. Dollimore and A. K. Galwey: *Comprehensive Chemical Kinetics*, Elsevier, Amsterdam 1980, Vol. 22.
20. G. Alberti and U. Costantino: in *Inclusion Compounds*, J. L. Atwood, J. E. D. Davies, and D. D. MacNicol (Eds.), Oxford University Press, Oxford, 1991, vol. 5, pp. 136–76.
21. J. Málek: unpublished results.